



Cost-effective liquid-junction solar devices with plasma-implanted Ni/TiN/CNF hierarchically structured nanofibers



Rugeng Liu^{a,b,1}, Xiang Peng^{c,d,1}, Xu Han^{a,b,1}, Chun Hong Mak^{a,b}, Kuan-Chen Cheng^{e,f,g,h}, Shella Permatasari Santoso^{i,j}, Hsin-Hui Shen^k, Qingdong Ruan^c, Fahe Cao^l, Edward T. Yu^m, Paul K. Chu^c, Hsien-Yi Hsu^{a,b,*}

^aSchool of Energy and Environment & Department of Materials Science and Engineering, City University of Hong Kong, Kowloon Tong, Hong Kong, China

^bShenzhen Research Institute of City University of Hong Kong, Shenzhen 518057, China

^cDepartment of Physics & Department of Materials Science and Engineering, City University of Hong Kong, Kowloon, Hong Kong, China

^dHubei Key Laboratory of Plasma Chemistry and Advanced Materials, School of Materials Science and Engineering, Wuhan Institute of Technology, Wuhan 430205, China

^eGraduate Institute of Food Science Technology, National Taiwan University, Taipei 10617, Taiwan, ROC

^fInstitute of Biotechnology, National Taiwan University, Taipei 10617, Taiwan, ROC

^gDepartment of Medical Research, China Medical University Hospital, China Medical University, Taichung, Taiwan, ROC

^hDepartment of Optometry, Asia University, 500, Lioufeng Rd., Wufeng, Taichung 41354, Taiwan, ROC

ⁱChemical Engineering Department, Widya Mandala Surabaya Catholic University, East Java, Indonesia

^jChemical Engineering Department, National Taiwan University of Science and Technology, Taipei, Taiwan, ROC

^kDepartment of Materials Science and Engineering, Faculty of Engineering, Monash University, Clayton, Victoria 3800, Australia

^lSchool of Materials, Sun Yat-sen University, Guanzhou 510006, China

^mMicroelectronics Research Center, Department of Electrical and Computer Engineering, the University of Texas at Austin, Austin, TX 78712, United States

ARTICLE INFO

Keywords:

Counter electrode
Photoelectrochemistry
Carbon materials

ABSTRACT

Carbon-based conductive materials have been recognized as promising alternatives to noble metals as the electrode in optoelectronic devices. Herein, by utilizing energetic plasma ion implantation, Ni-doped TiN nanowire (NWs) modified graphitic carbon nanofibers (CNF) are designed and prepared as the candidates of the platinum (Pt) counter electrode for low-cost hybrid perovskite-based liquid-junction photoelectrochemical solar cells (LPSCs). Notably, the photoelectrochemical (PEC) response of p-Rb_{0.05}FA_{0.95}PbI₃ based-LPSCs equipped with the Ni/TiN/CNF counter electrode is almost identical to that with a typical Pt counter electrode. From electrochemical investigations, i.e., electrochemical impedance spectroscopy (EIS), we observe that the CNF-based materials show a similar redox activity compared with the Pt counter electrode, indicating low charge-transfer resistance (R_{ct}) and large capacitance (C). The LPSCs, with a configuration of p-Rb_{0.05}FA_{0.95}PbI₃/BQ (2 mM), BQ^{•-} (2 mM)/Ni/TiN/CNF-based counter electrode, exhibit an open-circuit photovoltage of 1.00 V and a short-circuit current density of 7.02 mA/cm² under 100 mW/cm² irradiation. The overall optical-to-electrical energy conversion efficiency is 5.06%. The PEC solar cell shows good stability for 5 h under irradiation. The CNF-based counter electrode enables potential applications, including but not limited to PEC solar devices, dye-sensitized solar cells (DSSCs), solar fuel devices and hydrogen evolution reaction.

1. Introduction

Organic-inorganic hybrid perovskite materials have drawn extensive attention due to long exciton diffusion length, low excitation energy, tunable band gap and high absorption coefficient [1]. The power conversion efficiencies (PCEs) of the solid-state perovskite solar

cells (PSCs) have shown tremendous advancement within a decade [2]. However, the fabrication process for high-performance solid-state PSCs required complicated procedures, in which thermal evaporation technique is the necessity to deposit the organic and inorganic metal with high-quality and consistent layers. Moreover, large energy consumptions are required to fulfill the high temperature and vacuum

* Corresponding author at: School of Energy and Environment & Department of Materials Science and Engineering, City University of Hong Kong, Kowloon Tong, Hong Kong, China.
E-mail address: sam.hyhsu@cityu.edu.hk (H.-Y. Hsu).

¹ Contributing equally to this work.

operation condition in the thermal evaporating process. Liquid junction solar cell as one of the most cost-effective solar devices could provide a simplified structure of photovoltaic device in which the photoactive junction is formed by immersing the semiconductor in solution [3]. A typical hybrid perovskite-based liquid-junction photoelectrochemical solar cells (LPSCs) utilize three electrodes system, containing a photocathode, a counter electrode and a reference electrode immersed in an electrolyte containing redox couple of BQ/BQ⁻ (where BQ is benzoquinone) and tetrabutylammonium hexafluorophosphate (TBAPF₆) supporting electrolytes [3a]. It was demonstrated that the BQ/BQ⁻ redox couples exhibited relatively stable performance and suitable band gap in LPSC system compared with traditional redox couples, e.g. I₃⁻/I⁻ [3a]. The mixed cation perovskite, rubidium (Rb) and formamidinium (FA) lead iodide, was used as the light absorption layer due to its enhanced moisture-tolerance and photovoltaic performance proved by Park. et al. [4]. Thus, the Rb_{0.05}FA_{0.95}PbI₃ coated on transparent conducting substrate, usually fluorine-doped titanium oxide (FTO) glass, was adopted as the photocathode in this study. When the perovskite material exposed to sunlight, a photoelectron could be generated and the electrons transfer to the electrolyte, resulting in the reduction of BQ to BQ⁻. After the diffusion of BQ⁻ to the counter electrode surface, the reduced form of BQ is oxidized by losing electrons to the electrode surface. Pt is the most widely used counter electrode material in liquid junction cell, due to its efficient electrochemical activity for the oxidation and reduction reactions of BQ/BQ⁻. Nevertheless, the expensive cost and limited surface area of Pt counter electrodes may hinder the development of LPSCs.

With regards to low cost electrode materials, a series of carbon materials, such as carbon black, graphite, porous carbon, carbon nanotubes, were promising candidates which show comparable electrochemical properties with a representative Pt counter electrode [5]. In addition, the physical and chemical properties of carbon-based materials are satisfactory, leading to a competitive role in LPSCs [6]. Furthermore, the performance of electron transport on carbon materials can be improved by further increasing the contact area [7]. One-dimensional (1D) TiN have become new class of promising materials for electrochemical and photochemical applications because of excellent electrical conductivity for electron transport, high surface area of rough TiN for the deposition and/or doping of metal nanoparticles [8], as well as an outstanding physicochemical stability [9]. They have been already used as good conductors in dye-sensitized solar cell, fuel cell, and electrochemical capacitors [10]. Thus, the TiN-deposited carbon materials with a large surface area and fast charge transport will have a positive influence on improving the performance of LPSCs. To further improve the electrocatalytic performance, transition metal doping can be an effective way. Among all the transition metals, the Ni doping has attracted attention because of larger capacity, lower cost and non-toxicity compared to other heavy metals [11]. Parana et al. reported that the Ni-doped metal organic framework (MOF) involves an efficient and reversible Faradaic redox reaction between Ni(OH)₂ and NiO(OH)₂ in aqueous potassium hydroxide (KOH) electrolyte, efficaciously ameliorating the charge storage capability of the MOF [12]. On the other hand, Ni also played an important role in lithium-ion batteries to improve its output potential, energy density, power density and so on, due to their suitable electronic structure [13].

In terms of the doping techniques, plasma ion implantation can simultaneously dope metal ions and complete surface modification [14]. Positive and negative ions in plasma, i.e., charged and neutral particles, are exceptionally vigorous and thoroughly free to move [14a]. Accordingly, energetic ions in plasma exhibit an effectual chemical activity instead of diffusion-limited thermal reactions [15]. Plasma-assisted techniques have been developing into an influential implement for the modification of nanomaterials, due to the features of plasma, such as complexity, reactivity, and non-equilibrium. For the preparation process reacted under high temperatures, we could

consider to proceed them by a high-energy plasma technique with a short duration. The Metal Vapor Vacuum Arc (MEVVA) ion source with high current beams of metal ions is commonly employed among the diverse kinds of plasma techniques, in virtue of high energy efficiency, short treatment duration, as well as relatively low reactor-zone temperature, promoting the effectiveness of the surface reaction [16].

Herein, a cost-effectiveness carbon-based counter electrode for LPSCs we design in this report is a hybrid structure with large surface area and enhanced conductivity by Ni plasma ion implantation equipped with MEVVA ion source into 1D TiN NWs vertically coated onto the carbon nanofibers (CNF), as illustrated in Scheme 1. Based on the result of electrochemical studies, we confirm that the CNF materials counter electrodes present low charge-transfer resistance (R_{ct}), large capacitance (C), and fast reaction rates for BQ⁻ oxidation, implying that the CNF materials counter electrode can realize an efficient electrochemical reaction. As a result, the photovoltaic performance of CNF-based counter electrode on LPSCs, i.e., short circuit current density (J_{sc}), open circuit voltage (V_{oc}) and fill factor (FF), is firmly comparable in comparison to Pt-based solar devices.

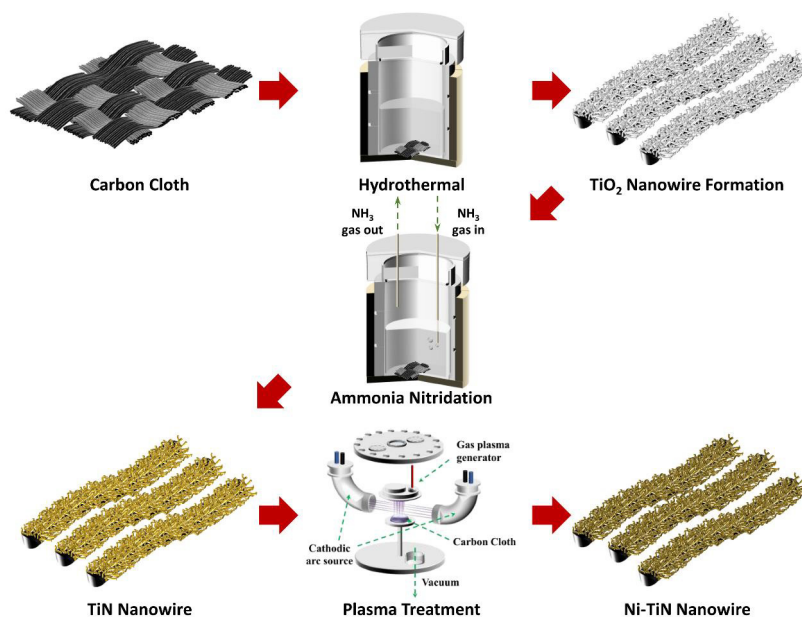
2. Experiment section

2.1. Preparation of TiN/CNF and Ni/TiN/CNF

The carbon nanofiber (CNF) used as the matrix material was bought from CeTech. A seed-assistant hydrothermal method was utilized for the preparation of TiO₂ NWs. The CNF was immersed in a titanium (IV) *n*-butoxide (TBT, 0.05 M, Sigma Aldrich) of ethanol solution for 40 min. Before hydrothermal reaction, the CNF was heated in the atmosphere at 400 °C for 30 min. The CNF with TiO₂ seeds was then put into a 50 mL Teflon container autoclave consisting of 15 mL acetone (RCI Labscan), 15 mL concentrated HCl (Sigma Aldrich) and 1.5 mL TBT. The autoclave was then put into an oven at 200 °C for 80 min. After cooling, washed and dried, the CNF with TiO₂ was prepared. The ammonia nitridation was used to convert the TiO₂/CNF to TiN/CNF at 900 °C for 2 h. The Ni ion implantation process was attained on a high-energy metal ion implanter (HEMII-80, Plasma Technology Ltd., Hong Kong SAR) using Ni as the target material with an accelerating voltage of 25 kV. The implantation fluence range was between 0.5×10^{16} and 3.0×10^{16} atoms cm⁻².

2.2. Characterization of CNF, TiN/CNF and Ni/TiN/CNF

The morphology and structure of the samples were investigated by scanning electron microscopy (SEM, FEI/Philips XL30 Esem-FEG) equipped with energy-dispersive X-ray spectroscopy (EDS). X-ray diffraction (XRD) spectra were collected at room temperature over a 2θ at certain range on PANalytical X-ray diffractometer (X'Pert3 Powder) using Cu-Kα radiation of 40 kV. The bonding structure was characterized at room temperature by high-resolution confocal Raman scattering (Horiba LAabRam HR VIS) with a 532 nm laser as the excitation source. Electrochemical impedance spectroscopy (EIS) measurements were carried out at the open-circuit potential (i.e., 0.5 V versus Ag/AgNO₃) in the dark using a CH Instruments model 760E electrochemical analyzer as a potentiostat with the AC impedance model. The AC signal had amplitude of 10 mV in the frequency range from 0.1 to 2×10^6 Hz at zero DC bias. Cyclic voltammetry (CV) experiments were performed using a Pt wire as counter electrode, a Ag/AgNO₃ as reference electrode, as well as a CNF material or Pt as working electrode in an CH₂Cl₂ solution containing 2 mM BQ/2 mM BQ⁻ using 0.1 M tetrabutylammonium hexafluorophosphate (TBAPF₆) as the supporting electrolyte at a potential scan rate of 100 mV s⁻¹.



Scheme 1. Schematic illustration of the fabrication process of the hierarchical Ni/TiN/CNF counter electrode.

2.3. Device fabrication and characterization

The $\text{Rb}_{0.05}\text{FA}_{0.95}\text{PbI}_3$ precursor solution was obtained by adding 5% of RbPbI_3 into FAPbI_3 precursor solution and stirred for 3 h at ambient temperature before use. The films for photoelectrochemical experiments were processed by the drop coating. The precursors were drop-coated on fluorine-doped tin oxide (FTO) glass substrates under annealing temperature at $100\text{ }^\circ\text{C}$ for 1.5 h directly.

The photoactivity of perovskites was measured in a photoelectrochemical cell. The prepared films were used as working electrodes (0.27 cm^2) exposed to electrolyte solution and irradiation. All measurements were carried out in a borosilicate glass cell with the $\text{Rb}_{0.05}\text{FA}_{0.95}\text{PbI}_3$ working electrode, a carbon-based counter electrode and Ag/AgNO_3 reference electrode (a silver wire immersed in 0.01 M silver nitrate in MeCN connected to the cell via a 0.10 M TBAPF_6 in CH_2Cl_2 salt bridge). UV-vis light was irradiated through the electrolyte solution using full output of the Xe lamp with an incident light intensity of about $100\text{ mW}/\text{cm}^2$. The supporting electrolyte was 0.1 M TBAPF_6 in CH_2Cl_2 . The IPCE was measured through a monochromator (Photon Technology International, Birmingham, NJ) in combination with a power meter (model 1830-C, Newport, Irvine, CA) and a silicon detector (model 818-UV, Newport, Irvine, CA).

3. Results and discussion

3.1. Material design and characterization

The construction of the hierarchical Ni/TiN/CNF counter electrodes by surface modification and interfacial engineering is depicted in Scheme 1. Through the hydrothermal reaction as well as NH_3 treatment, the TiN NWs were grown on the surface of carbon nanofibers. Following the preparation of TiN/CNF, Ni is plasma ion implanted to dope and amorphize the surface of the TiN NWs. The hierarchically structured Ni/TiN/CNF through this stage-by-stage procedure was obtained. As shown in Fig. 1a and 1d, the SEM images indicate the smooth surface of commercial CNFs. Meanwhile, the SEM images in Fig. 1b and 1e show a rough morphology which belongs to the CNFs with dense vertical TiN NWs after hydrothermal and NH_3 treatment. According to material characterization, the NWs can be identified as TiN determined by XRD in Fig. 2a. We demonstrate that the TiN NWs have been grown on CNFs (i.e., TiN/CNF), and the surface area

with rough morphology is attained by an introduction of TiN NWs. Moreover, it was reported that TiN on the carbon substrate possessed the enhanced metallic behaviors, such as good electrical conductivity, giving rise to the improvement of charge transport efficiency because of high conductivity of TiN NWs [8a]. In addition, more active sites for electrochemical activity were produced due to the rough TiN NWs. Interestingly, by using Ni plasma ion implantation, the change of the hierarchical structure is not distinct, as displayed in Fig. 1c and f.

After the plasma ion implantation, no signal corresponding to Ni species is observed in XRD spectra, while the signals from the TiN and CNF substrate is shown in the XRD pattern (Fig. 2a). But by utilizing energy dispersive X-ray spectrometry (EDS) depicted in Fig. 2 (c-d) as well as the EDS mapping in Fig. S1, after Ni plasma ion implantation onto the TiN/CNF, a small amount of Ni doped onto the TiN/CNF is detected to confirm the construction of the Ni/TiN/CNF hierarchical structure. Raman spectroscopy has been widely used to explore the microstructure of carbonaceous materials, along with vibrational and rotational interactions between molecules [17]. This technique is responsive not only to the crystal structure, but also to the structural changes at molecular level. In Fig. 2b, two typical bands of carbonaceous materials (i.e., D-band and G-band) centered at the wavenumber of $\sim 1330\text{ cm}^{-1}$ and 1585 cm^{-1} are related to disordered and/or turbostratic carbonaceous components, as well as the ordered graphitic structures, respectively [17d]; D band and G-band are ascribed to the A_{1g} and E_{2g2} modes, indicating out-of-plane and in-plane C=C stretching vibrations of graphite crystallites [18]. The amount of structurally ordered graphite crystallites in the carbonaceous materials can be determined by the intensity ratio of the D-band to the G-band, known as the *R*-value [17d,19]. The *R*-values of non-modified CNF is 1.22, while the *R*-values decrease to 1.18 and 0.96 separately after the loading of TiN and further Ni-ions plasma doping process (Table S1). It is conspicuous that the *R*-value of carbon nanofiber was decreased with a TiN-modified process, as a result of partial conversion from disordered carbonaceous components into the ordered graphite crystallites. By utilizing Ni plasma ion implantation, the order of the graphite crystallinity has been further increased.

3.2. Electrochemistry

To verify the availability of CNF, TiN/CNF and Ni/TiN/CNF as the counter electrode in LPSCs, cyclic voltammograms (CV) were

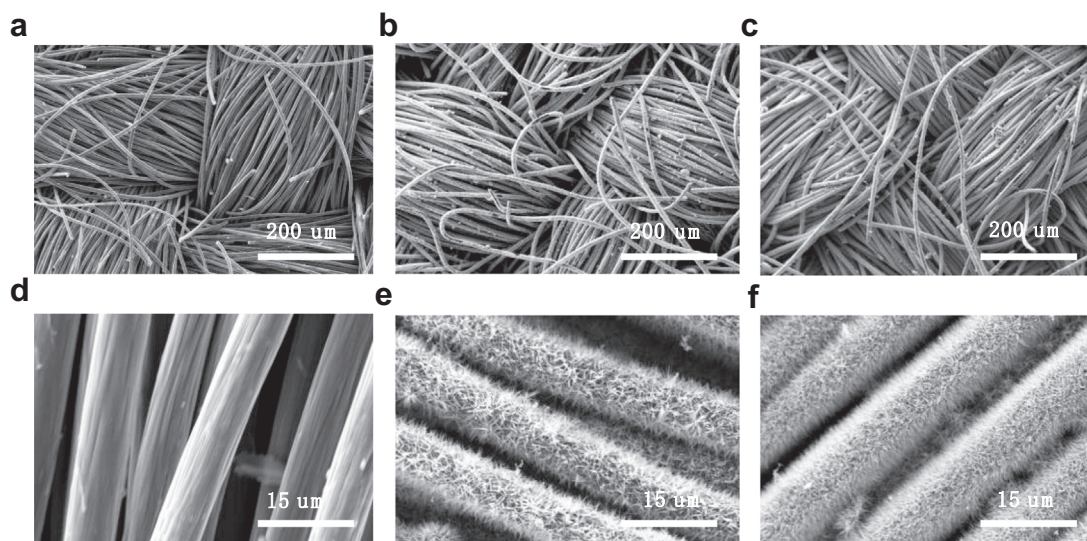


Fig. 1. SEM images of (a and d) CNF, (b and e) TiN/CNF, and (c and f) Ni/TiN/CNF.

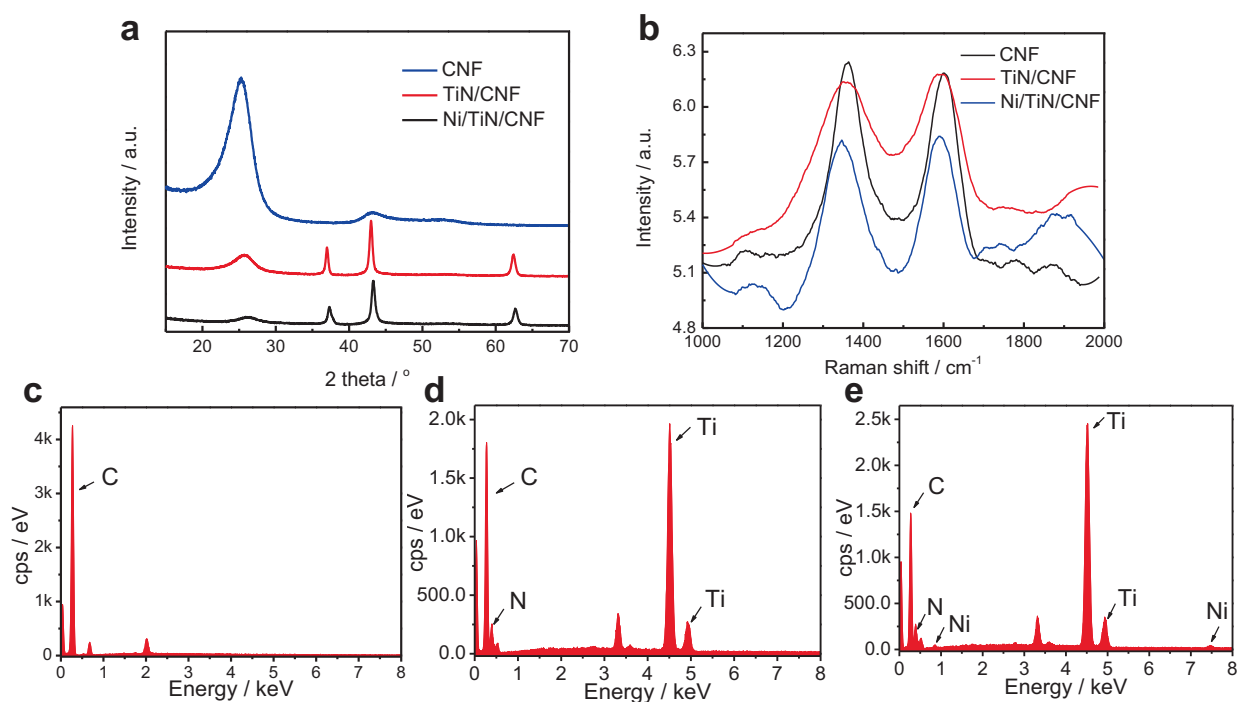


Fig. 2. (a) XRD patterns of CNF, TiN/CNF and Ni/TiN/CNF; (b) Raman shift of CNF, TiN/CNF and Ni/TiN/CNF; EDS spectrums of (c) CNF, (d) TiN/CNF, and (e) Ni/TiN/CNF.

performed for carbonaceous materials compared with platinum (Pt) containing 2 mM BQ/BQ⁻ using 0.1 M tetrabutylammonium hexafluorophosphate (TBAPF₆) as the supporting electrolyte, as shown in Fig. 3a. The Pt electrode with the exposed area (~1.0 cm²) exhibits evident reduction and oxidation behavior, showing peak splitting with the first wave at approximately -0.90 V and the second at around -0.65 V (formal potential = -0.775 vs Ag/AgNO₃). However, there is only an anodic shoulder at ca. -0.5 V observed for the CNF electrode with the same exposed area. For TiN/CNF and Ni/TiN/CNF electrodes, the current densities are dominated by the double layer capacitive charging current. Furthermore, the irreversible reduction peaks are observed for TiN/CNF and Ni/TiN/CNF electrodes, indicating that TiN/CNF and Ni/TiN/CNF are relatively

unstable in this system. On the basis of the CV measurements, Ni doped TiN/CNF (Ni/TiN/CNF) is a relatively effective counter candidate compared to TiN/CNF. More electrochemical and photoelectrochemical characterizations are provided below to confirm the availability of modified carbonaceous materials as the potential counter electrodes in LPSCs. A representative PEC system mainly involves one working electrode (Rb_{0.05}FA_{0.95}PbI₃ hybrid perovskite film on the top of an FTO substrate) for the production and detection of reduced species, and the counter electrode (i.e., Pt-wire, CNF, TiN/CNF or Ni/TiN/CNF) to generate an oxidized mediator species O_x at a diffusion-limited rate from a reduced species which are formed by the working electrode in the electrolyte. The PEC responses of Pt, CNF, TiN/CNF and Ni/TiN/CNF for BQ redox reaction were

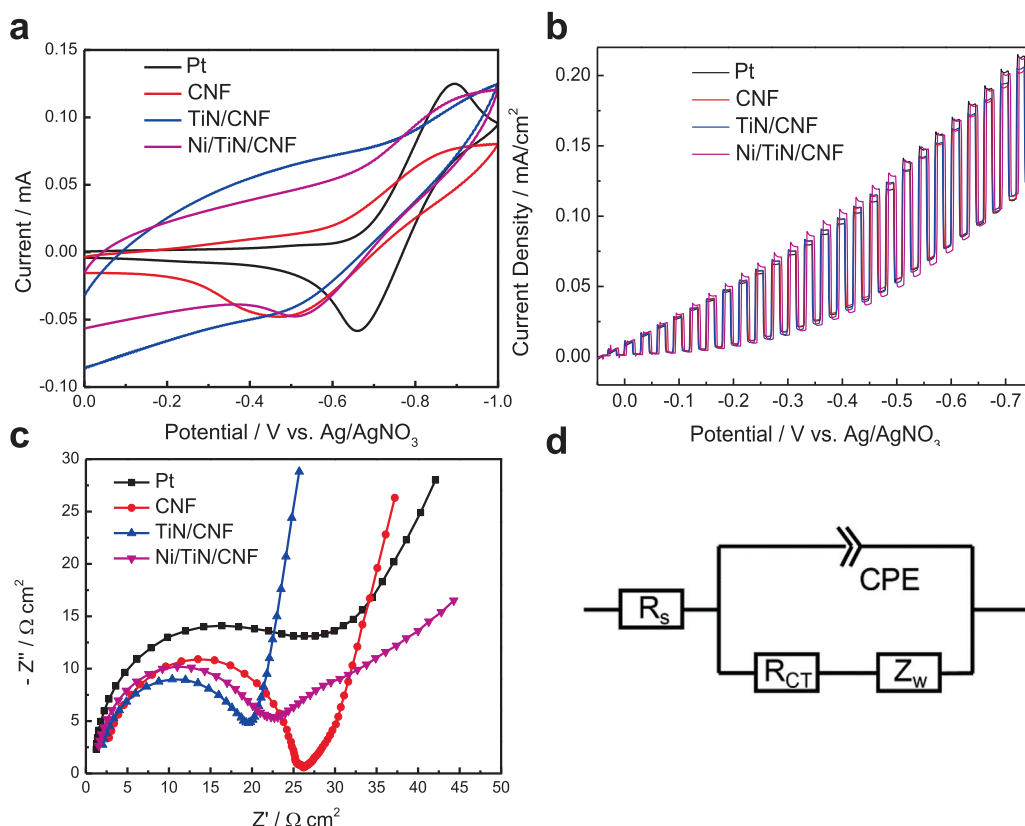


Fig. 3. (a) Cyclic voltammograms of Pt-wire (black), CNF (red), TiN/CNF (blue) and Ni/TiN/CNF (magenta) electrodes in an CH₂Cl₂ solution containing 2 mM BQ and BQ^{•-} using 0.1 M TBAPF₆ as the supporting electrolyte. The reference electrode was 0.01 M. Ag/AgNO₃; (b) LSV characteristics for different counter electrode: Pt (black), CNF (red), TiN/CNF (blue) and Ni/TiN/CNF (magenta) under chopped illumination; (c) Nyquist plots of electrode cell by different counter electrode: Pt (black), CNF (red), TiN/CNF (blue) and Ni/TiN/CNF (magenta) (d) equivalent circuit of the electrochemical.

characterized by linear sweep voltammetry (LSV) with chopped light under irradiation. The LSV of Pt, CNF, TiN/CNF and Ni/TiN/CNF counter electrode was conducted from +0.05 V to -0.70 V vs Ag/AgNO₃ at a scan rate of 10 mV/s (Fig. 3b). All the counter electrodes were active in the oxidation of BQ^{•-}, and the Rb_{0.05}FA_{0.95}PbI₃ hybrid perovskite exhibited a well-defined p-type behavior with onset potential at -0.05 V. The Rb_{0.05}FA_{0.95}PbI₃ using the Pt counter electrode under a PEC system shows the highest photocurrent of 0.103 mA/cm² at -0.7 V vs Ag/AgNO₃, while that perovskite with TiN/CNF or CNF counter electrodes generated the photocurrents of 0.091 or 0.090 mA/cm² at -0.7 V vs Ag/AgNO₃, respectively. The dark current of hybrid perovskites in LPSCs was almost no change after 10 days. The degradation of PEC performance for hybrid perovskite-based LPSCs was much slower (<5%) for the films stored under 0% RH and 50% RH after 30 days of exposure. In terms of Ni/TiN/CNF counter electrode, the PEC response was increased to 0.097 mA/cm² at -0.7 V vs Ag/AgNO₃. Therefore, carbonaceous materials are definitely potential candidates to replace Pt materials in LPSCs.

The electrochemical reactivity and catalytic performance of counter electrodes are generally evaluated by utilizing the electrochemical impedance spectroscopy (EIS) [20]. An electrochemical cell used for EIS characterization contains the carbonaceous material (i.e., CNF, TiN/CNF or Ni/TiN/CNF) and a Pt wire as the electrode. Fig. 3c reveals the Nyquist plots of carbonaceous materials and Pt electrode. An equivalent circuit diagram applied in electrochemical impedance spectroscopy is illustrated in Fig. 3d. For carbonaceous materials or a Pt wire, the charge transfer resistance (R_{ct}) at the electrode-electrolyte interface, series resistance (R_s), constant phase element (CPE), as well as Warburg impedance (Z_w) are included in the circuit elements [21]. The charge transfer process at the electrode-electrolyte

interface results in the high-frequency semicircle, while the Nernst diffusion impedance (Z_w) of the redox couple in the electrolyte leads to the low frequency arc [22]. Table 1 shows the results of the Nyquist plots fitted based on the equivalent circuit diagram. The charge transfer resistances (R_{ct}) of the CNF and TiN/CNF electrode is found to be 23.86 Ω cm² and 18.88 Ω cm² respectively. After doping of Ni onto TiN/CNF, the R_{ct} decreased to 18.22 Ω cm², which were less than that (27.12 Ω cm²) of the Pt-wire electrode; in other words, carbonaceous material exhibit relatively high electrochemical performance. Noticeably, based on the equivalent circuit diagram, the semi-circle diameter is affected by two factors, i.e., charge-transfer resistance (R_{ct}) of semi-conductors and the diffusion impedance (Z_w).

The capacitance at the interface between the electrode (i.e., carbonaceous materials or a Pt wire) and the electrolyte is determined by the CPE, depicting as

$$Z_{CPE} = \frac{1}{Y_0} (j\omega)^{-\beta}$$

where Y₀ is the CPE parameter, β is the CPE exponent (0 < β < 1), and ω is the angular frequency. Both Y₀ and β are independent of frequency.

The exact semicircle with a β value of 1 represents an ideal capacitance. Nevertheless, the depression from a semicircle into an ellipse in the Nyquist plots gives rise to a non-ideal capacitance at the interface between counter electrode and electrolyte, arising from several factors consisting of porous films, surface roughness, leaky capacitor, and non-uniform current distribution [20a,21], characteristically resulting in a decline of the β value down to lower than 1. According to fitted results listed in Table 1, the β values of the CNF, TiN/CNF and Ni/TiN/CNF counter electrodes were 0.97, 0.96 and 0.96 respectively, which were smaller than the Pt electrode with a β value of 0.99. The

Table 1
Fitted Parameters Extracted from the Nyquist Plots of the Respective CNF materials and Pt-wire Counter Electrode.

Counter electrode	$R_s(\Omega \text{ cm}^2)$	$R_{ct}(\Omega \text{ cm}^2)$	$C(\mu\text{F cm}^{-2})$	β
Pt	0.96	27.12	69.5	0.99
CNF	2.01	23.86	85.8	0.97
TiN/CNF	1.43	18.88	88.9	0.96
Ni/TiN/CNF	1.01	18.22	86.3	0.96

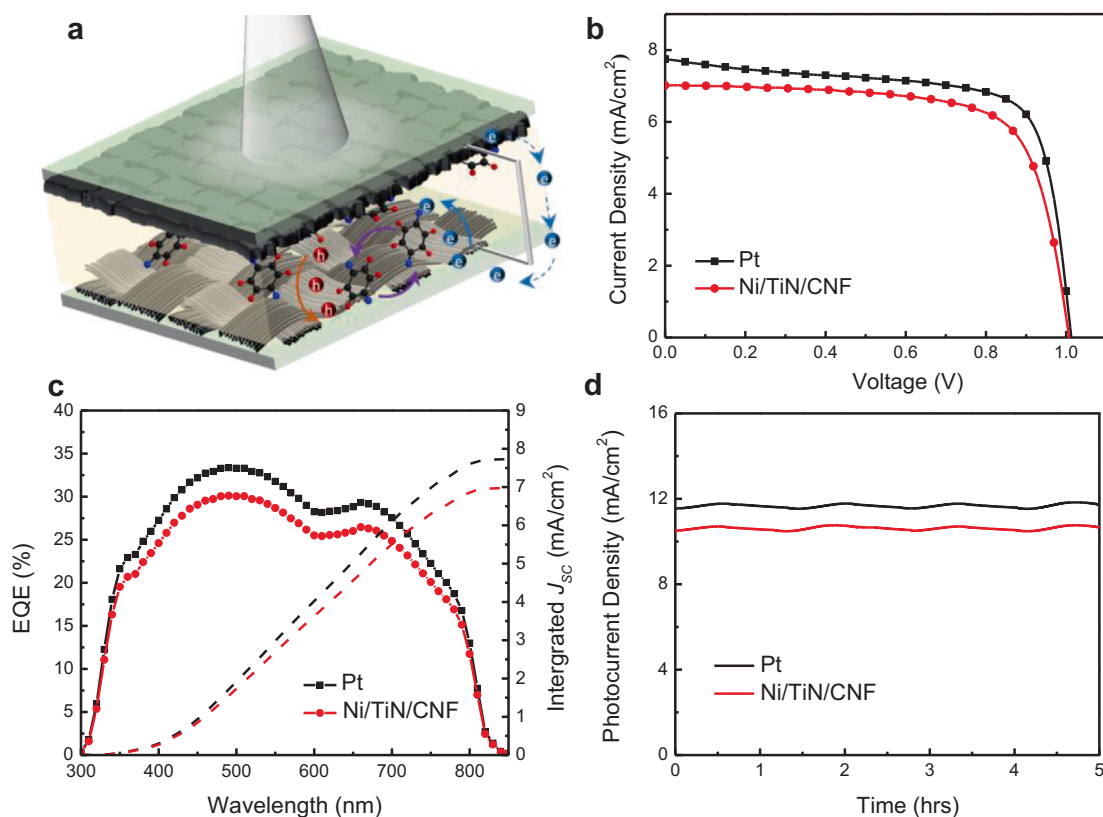


Fig. 4. (a) Schematic illustration of LPSCs containing a $\text{Rb}_{0.05}\text{FA}_{0.95}\text{PbI}_3$ perovskite photocathode, as well as the Pt or carbonaceous counter electrodes (b) Steady-state current density–voltage relation for a $\text{p-Rb}_{0.05}\text{FA}_{0.95}\text{PbI}_3/\text{BQ}$ (2 mM), BQ^- (2 mM)/CE LPSCs under irradiation with a 100 mW/cm^2 Xe lamp focused onto the photoelectrode. The optical path through the solution was about 0.3 mm; (c) External quantum efficiency (EQE) spectra and integrated J_{sc} values of Pt and Ni/TiN/CNF-based LPSCs; (d) Time dependence of the photocurrent of a $\text{p-Rb}_{0.05}\text{FA}_{0.95}\text{PbI}_3/\text{BQ}$ (2 mM), BQ^- (2 mM)/CE PEC cell at -0.6 V . The $\text{p-Rb}_{0.05}\text{FA}_{0.95}\text{PbI}_3$ photoelectrode was irradiated by a 150 mW/cm^2 Xe lamp. The optical path through the solution was about 0.3 mm.

lower β value indicates that the surface roughness of CNF counter electrodes is higher than that of the Pt counter electrode [21]. Moreover, the capacitance (C) of CNF electrodes is larger than that of the Pt electrode, implying that carbonaceous electrodes manifest a larger surface area. Such result is consistent with previous report that nanostructured counter electrodes with a high porosity shows a higher capacitance [21,22b,22c]. It is clearly observed that the Ni/TiN/CNF electrode possesses larger capacitance ($86.3 \mu\text{F cm}^{-2}$) than Pt electrode. However, the series resistance of the CNF counter electrodes by the fitting model distributed from $1.01 \Omega \text{ cm}^2$ to $2.01 \Omega \text{ cm}^2$, which were more than two times of $0.96 \Omega \text{ cm}^2$ for the Pt electrode, probably due to an increased film thickness of carbonaceous materials compared to that of the Pt electrode [21], as well as a higher Nernst diffusion impedance (Z_w) of benzoquinone ions [23]. Among these CNF counter electrodes, the Ni/TiN/CNF material still shows the lowest series resistance. This is possibly attributed to apparent enhancement of graphite content and conductivity for the Ni/TiN/CNF materials. Further investigation on the capacitance and/or pseudocapacitance in organic solutions is of importance to elucidate the electron transfer mechanism in the complex electrochemical system.

3.3. Photovoltaic performance

The LSV result provides a guidance for the fabrication of LPSCs, where the open-circuit potential of photovoltaic materials without recombination processes is theoretically close to ΔV . According to relatively efficient PEC activity of $\text{p-Rb}_{0.05}\text{FA}_{0.95}\text{PbI}_3$ perovskites with different counter electrodes, the experimental performance for two-electrode photovoltaic devices is significant because the responses are not produced by conductivity changes upon solar illumination. Based on the electrochemical characterization, the photovoltaic behavior of the potential counter electrode, Ni/TiN/CNF, was then investigated in the LPSCs, as shown in Fig. 4a. The perovskite photocathode as well as a Pt or Ni/TiN/CNF counter electrode, were spaced about 0.3 mm apart with a Teflon gasket, with perovskite material about $<1 \text{ mm}$ away from the cell window. The current density–voltage (J - V) curves of LPSCs with Pt or Ni/TiN/CNF counter electrode are performed under AM 1.5 solar simulator illumination at 100 mW cm^{-2} , as shown in Fig. 4b. The LPSC with a Pt counter electrode show a J_{sc} of 7.75 mA cm^{-2} , V_{oc} of 1.01 V, and fill factor (FF) of 72.4%, generating a rational power conversion efficiency (η) of 5.67%. On the

other hand, the LPSCs with the Ni/TiN/CNF counter electrode exhibits a satisfactory performance with a J_{sc} of 7.02 mA cm^{-2} , V_{oc} of 1.00 V , and fill factor (FF) of 72.1% . The V_{oc} of Ni/TiN/CNF-based LPSCs is almost identical to that of Pt-based solar devices; however, the J_{sc} of Ni/TiN/CNF-based devices is slightly lower than that of the Pt-based LPSCs. In addition to the decreased J_{sc} , the FF was reduced by the increase of the series resistance (R_s) in Ni/TiN/CNF based LPSCs, leading to relatively lower η [24].

The photocurrent for the p-Rb_{0.05}FA_{0.95}PbI₃ in the $2 \text{ mM BQ}^-/\text{BQ}$ system was measured as a function of wavelength over the range from 300 to 850 nm using a Xe lamp. External quantum efficiency (EQE) spectra of the devices and integrated J_{sc} for the Ni/TiN/CNF- and Pt-based LPSCs were calculated and are plotted in Fig. 4c. They reach the maxima of 30.33% and 33.45% at 490 nm and gradually declined at longer wavelength, directly pointing out that the LPSCs with a Ni/TiN/CNF counter electrode exhibit slightly lower EQE than that with the Pt electrode over the wavelength range. This is most likely because unabsorbed incident light was reflected back to the perovskite photocathode for re-absorption by the Pt counter electrode, giving rise to an increased J_{sc} [23a,25]. In general, such a reflection effect cannot be elicited by the carbonaceous counter electrode, e.g., Ni/TiN/CNF. Integration of the EQE spectra gives current densities of approximately 7.72 mA/cm^2 and 7.00 mA/cm^2 , and there is a good agreement with the current density measured using the solar simulator. The hybrid perovskite film still retained more than 95% of the initial UV-Vis absorption after 37 days of exposure. The photocurrent as a function of time is shown in Fig. 4d. The photocurrent was stable for five hours, at which time the experiment was terminated under irradiation at the higher power intensity (150 mW/cm^2).

4. Conclusion

In summary, a novel counter electrode material for cost-effective and efficient LPSC was developed by modify the CNF using TiN and plasma process. The TiN was successfully deposited on the CNF to form the nanowire morphology and the Ni iron was implanted into the TiN/CNF. The CNF-based counter electrode, especially the Ni/TiN/CNF counter electrode show a comparable electrochemistry activity with Pt counter electrode as demonstrated with photovoltaic and photoelectrochemical investigations, i.e., low charge-transfer resistance (R_{ct}), large capacitance, and fast reaction rates for oxygen of BQ^- ions between counter electrode and electrolyte. That is attributed to the larger specific surface area and significantly higher electrochemical performance. As a result, compared to LPSC device with Pt counter electrode, the Ni/TiN/CNF based cells exhibited a reasonable η up to 5.06% under the AM 1.5 illumination at 100 mW cm^{-2} , with nearly the same open circuit voltage (V_{oc}) as well as commensurable fill factor (FF) and current density (J_{sc}). It is envisioned that Ni/TiN/CNF can serve as an economic alternative as a counter electrode material in LPSCs as compared to conventional Pt metals. The low-cost, easy to scale-up and efficient fabrication process of Ni/TiN/CNF counter electrode is conducive to the industrialization of LPSCs. Significantly, the newly developed Ni/TiN/CNF opens up an avenue for high-performance energy conversion and storage devices, including but not limited to Li-ion battery, dye sensitize solar cell, supercapacitor and fuel cells.

Conflicts of interest

There are no conflicts to declare.

CRediT authorship contribution statement

R. L., X. H. and H.-Y.H. contributed to the design concept. R. L., X. P., X. H., C. H. M. and Q. R. performed the fabrication process and

measurements. All authors discussed the results and commented on the manuscript.

Declaration of Competing Interest

The authors declare that they have no known competing financial interests or personal relationships that could have appeared to influence the work reported in this paper.

Acknowledgements

The authors acknowledge financial support from the Research Grants Council of Hong Kong (Grant No. 21203518, F-CityU106/18 and 9048121), City University of Hong Kong (Grant No. 7005289, 7005580, 9680208, 9667213 and 9052029), as well as Shenzhen Science Technology and Innovation Commission (Grant No. R-IND12302).

Appendix A. Supplementary data

Supplementary data to this article can be found online at <https://doi.org/10.1016/j.jelechem.2021.115167>.

References

- [1] (a) G. Xing, N. Mathews, S. Sun, S.S. Lim, Y.M. Lam, M. Grätzel, S. Mhaisalkar, T. C. Sum, *Science* 342 (2013) 344–347; (b) S.S. Shin, J.H. Suk, B.J. Kang, W. Yin, S.J. Lee, J.H. Noh, T.K. Ahn, F. Rotermund, I.S. Cho, S.I. Seok, *Energy Environ. Sci.* 12 (2019) 958–964; (c) H.-Y. Hsu, L. Ji, M. Du, J. Zhao, T.Y. Edward, A.J. Bard, *Electrochim. Acta* 220 (2016) 205–210; (d) Z. Chen, H.-Y. Hsu, M. Arca, K.S. Schanze, *J. Phys. Chem. B* 119 (2014) 7198–7209; (e) C.H. Mak, X. Huang, R. Liu, Y. Tang, X. Han, L. Ji, X. Zou, G. Zou, H.-Y. Hsu, *Nano Energy* (2020); (f) D. Luo, W. Yang, Z. Wang, A. Sadhanala, Q. Hu, R. Su, R. Shivanna, G.F. Trindade, J.F. Watts, Z. Xu, *Science* 360 (2018) 1442–1446; (g) M. Saliba, J.P. Correa-Baena, M. Grätzel, A. Hagfeldt, A. Abate, *Angew. Chem. Int. Ed.* 57 (2018) 2554–2569.
- [2] (a) E.H. Jung, N.J. Jeon, E.Y. Park, C.S. Moon, T.J. Shin, T.-Y. Yang, J.H. Noh, J. Seo, *Nature* 567 (2019) 511; (b) Y. Tang, C.H. Mak, R. Liu, Z. Wang, L. Ji, H. Song, C. Tan, F. Barrière, H.Y. Hsu, *Adv. Funct. Mater.* (2020) 2006919; (c) R. Liu, C.H. Mak, X. Han, Y. Tang, G. Jia, K.-C. Cheng, H. Qi, X. Zou, G. Zou, H.-Y. Hsu, *J. Mater. Chem. A* 8 (2020) 23803–23811.
- [3] (a) H.-Y. Hsu, L. Ji, H.S. Ahn, J. Zhao, E.T. Yu, A.J. Bard, *J. Am. Chem. Soc.* 137 (2015) 14758–14764; (b) S. Rao, X. Zou, S. Wang, T. Shi, Y. Lu, L. Ji, H.-Y. Hsu, Q. Xu, X. Lu, *J. Electrochem. Soc.* 166 (2019) D427; (c) H.-Y. Hsu, L. Ji, C. Zhang, C.H. Mak, R. Liu, T. Wang, X. Zou, S.-Y. Leu, T.Y. Edward, *J. Mater. Chem. C* 6 (2018) 11552–11560; (d) J. Zhao, H. Yin, T. Lim, H. Xie, H.-Y. Hsu, F. Forouzan, A.J. Bard, *J. Electrochem. Soc.* 163 (2016) D506–D514.
- [4] Y.H. Park, I. Jeong, S. Bae, H.J. Son, P. Lee, J. Lee, C.H. Lee, M.J. Ko, *Adv. Funct. Mater.* 27 (2017) 1605988.
- [5] (a) Z. Liu, M. Zhang, X. Xu, L. Bu, W. Zhang, W. Li, Z. Zhao, M. Wang, Y.-B. Cheng, H. He, *Dalton Trans.* 44 (2015) 3967–3973; (b) D. Perganti, M. Giannouri, A.G. Kontos, P. Falaras, *Electrochim. Acta* 232 (2017) 517–527; (c) G. Volonakis, M.R. Filip, A.A. Haghighirad, N. Sakai, B. Wenger, H.J. Snaith, F. Giustino, *J. Phys. Chem. Lett.* (2016); (d) C.-S. Wu, T.-W. Chang, H. Teng, Y.-L. Lee, *Energy* 115 (2016) 513–518; (e) J.-Z. Chen, C. Wang, C.-C. Hsu, I.-C. Cheng, *Carbon* 98 (2016) 34–40; (f) A.K. Baranwal, S. Kanaya, T.N. Peiris, G. Mizuta, T. Nishina, H. Kanda, T. Miyasaka, H. Segawa, S. Ito, *ChemSusChem* 9 (2016) 2604–2608; (g) A. Sahasrabudhe, S. Kapri, S. Bhattacharyya, *Carbon* 107 (2016) 395–404.
- [6] E. Ramasamy, W.J. Lee, D.Y. Lee, J.S. Song, *Appl. Phys. Lett.* 90 (2007) 173103.
- [7] (a) H. Vrubel, T. Moehl, M. Grätzel, X. Hu, *Chem. Commun.* 49 (2013) 8985–8987; (b) T.-H. Lai, I. Constantinou, C.M. Grand, E.D. Klump, S. Baek, H.-Y. Hsu, S.-W. Tsang, K.S. Schanze, J.R. Reynolds, *F. So. Chem. Mater.* 28 (2016) 2433–2440; (c) S. Liu, Q. Zhang, L. Zhang, L. Gu, G. Zou, J. Bao, Z. Dai, *J. Am. Chem. Soc.* (2016).
- [8] (a) Y. Xie, C. Xia, H. Du, W. Wang, *J. Power Sources* 286 (2015) 561–570; (b) X. Peng, A.M. Qasim, W. Jin, L. Wang, L. Hu, Y. Miao, W. Li, Y. Li, Z. Liu, K. Huo, *Nano Energy* 53 (2018) 66–73.
- [9] G. Liu, Z. Pan, B. Zhang, J. Xiao, G. Xia, Q. Zhao, S. Shi, G. Hu, C. Xiao, Z. Wei, *Int. J. Hydrogen Energy* 42 (2017) 12467–12476.

- [10] (a) Q. Jiang, G. Li, X. Gao, *Chem. Commun.* (2009) 6720–6722;
(b) D. Choi, P.N. Kumta, *J. Electrochem. Soc.* 153 (2006) A2298–A2303.
- [11] T. Kawaguchi, K. Fukuda, K. Tokuda, M. Sakaida, T. Ichitsubo, M. Oishi, J.i. Mizuki, E. Matsubara, *Phys. Chem. Chem. Phys.* 17 (2015) 14064–14070.
- [12] P.C. Banerjee, D.E. Lobo, R. Middag, W.K. Ng, M.E. Shaibani, M. Majumder, *ACS Appl. Mater. Interfaces* 7 (2015) 3655–3664.
- [13] W. Liu, P. Oh, X. Liu, M.J. Lee, W. Cho, S. Chae, Y. Kim, J. Cho, *Angew. Chem. Int. Ed.* 54 (2015) 4440–4457.
- [14] (a) Y. Zhang, B. Ouyang, J. Xu, S. Chen, R.S. Rawat, H.J. Fan, *Adv. Energy Mater.* 6 (2016) 1600221;
(b) Y. Zhang, R.S. Rawat, H.J. Fan, *Small Methods* 1 (2017) 1700164;
(c) S. Dou, L. Tao, R. Wang, S. El Hankari, R. Chen, S. Wang, *Adv. Mater.* 30 (2018) 1705850.
- [15] (a) Q. Jiang, N. Chen, D. Liu, S. Wang, H. Zhang, *Nanoscale* 8 (2016) 11234–11240;
(b) I. Constantinou, T.H. Lai, H.Y. Hsu, S.H. Cheung, E.D. Klump, K.S. Schanze, S. K. So, F. So, *Adv. Electr. Mater.* 1 (2015) 1500167.
- [16] I. Brown, J. Washburn, *Nucl. Instruments Methods Phys. Res. Sect. B* 21 (1987) 201–204.
- [17] (a) N. Melanitis, P. Tetlow, C. Galiotis, *J. Mater. Sci.* 31 (1996) 851–860;
(b) J. Mittal, O. Bahl, R. Mathur, *Carbon* 8 (1997) 1196–1197;
(c) M. Endo, C. Kim, T. Karaki, T. Kasai, M. Matthews, S. Brown, M. Dresselhaus, T. Tamaki, Y. Nishimura, *Carbon* 36 (1998) 1633–1641;
(d) T. Jawhari, A. Roid, J. Casado, *Carbon* 33 (1995) 1561–1565.
- [18] R. Baddour-Hadjean, J.-P. Pereira-Ramos, *Chem. Rev.* 110 (2009) 1278–1319.
- [19] S.L. Rebelo, A. Guedes, M.E. Szczyk, A.M. Pereira, J.P. Araújo, C. Freire, *Phys. Chem. Chem. Phys.* 18 (2016) 12784–12796.
- [20] (a) A. Hauch, A. Georg, *Electrochim. Acta* 46 (2001) 3457–3466;
(b) G. Wang, W. Xing, S. Zhuo, *Electrochim. Acta* 92 (2013) 269–275;
(c) M. Wu, X. Lin, A. Hagfeldt, T. Ma, *Chem. Commun.* 47 (2011) 4535–4537.
- [21] T.N. Murakami, S. Ito, Q. Wang, M.K. Nazeeruddin, T. Bessho, I. Cesar, P. Liska, R. Humphry-Baker, P. Comte, P. Péchy, *J. Electrochem. Soc.* 153 (2006) A2255–A2261.
- [22] (a) X. Mei, S.J. Cho, B. Fan, J. Ouyang, *Nanotechnology* 21 (2010);
(b) G.R. Li, F. Wang, Q.W. Jiang, X.P. Gao, P.W. Shen, *Angew. Chem. Int. Ed.* 49 (2010) 3653–3656;
(c) Q. Jiang, G. Li, S. Liu, X. Gao, *J. Phys. Chem. C* 114 (2010) 13397–13401;
(d) M. Wang, A.M. Anghel, B. Marsan, N.-L. Cevey Ha, N. Pootrakulchote, S.M. Zakeeruddin, M. Grätzel, *J. Am. Chem. Soc.* 131 (2009) 15976–15977.
- [23] (a) S. Bai, C. Bu, Q. Tai, L. Liang, Y. Liu, S. You, Z. Yu, S. Guo, X. Zhao, *ACS Appl. Mater. Interfaces* 5 (2013) 3356–3361;
(b) S. An, Y.I. Kim, H.S. Jo, M.-W. Kim, M.W. Lee, A.L. Yarin, S.S. Yoon, *Chem. Eng. J.* 327 (2017) 336–342.
- [24] (a) D.-Y. Kang, Y. Lee, C.-Y. Cho, J.H. Moon, *Langmuir* 28 (2012) 7033–7038;
(b) G. Zhu, L. Pan, T. Xu, Z. Sun, *ACS Appl. Mater. Interfaces* 3 (2011) 1472–1478;
(c) I.J. Junger, C. Großerhode, J.L. Storck, S. Kohn, T. Grethe, C. Grassmann, A. Schwarz-Pfeiffer, N. Grimmelsmann, H. Meissner, T. Blachowicz, *Optik* 174 (2018) 40–45.
- [25] (a) J.V. Patil, S.S. Mali, A.S. Kamble, C.K. Hong, J.H. Kim, P.S. Patil, *Appl. Surf. Sci.* 423 (2017) 641–674;
(b) G.H. Kim, S.H. Park, M.S. Birajdar, J. Lee, S.C. Hong, *J. Ind. Eng. Chem.* 52 (2017) 211–217.